Acta Geotechnica (2016) 11:625–642
DOI 10.1007/s11440-016-0445-9

RESEARCH PAPER

A large-scale excavation in soft Holocene deposit and its elasto-viscoplastic analysis

Fusao Oka[1] · Naoki Takada[2] · Kazuyuki Shimono[3] · Yosuke Higo[4] · Sayuri Kimoto[5]

Received: 25 December 2014 / Accepted: 2 February 2016 / Published online: 2 March 2016

Abstract In the present study, the large-scale excavation in the construction is numerically back-analyzed using a soil–water-coupled finite element method with an elasto-viscoplastic model which considers the strain-induced degradation. The measurements of the deformation have been performed during the construction of a new railway station in Osaka, Japan, in which a large and deep excavation has been successfully carried out using a special deep mixing type of soil improvement method with earth retaining walls through the thick Holocene Osaka Umeda clay deposit. A comparison between the numerical results and the measurements of the excavation at Osaka shows that the simulation method can reproduce the overall deformation of the soft ground and the earth retaining walls including the time-dependent behaviour during the excavation and a deep mixing soil improvement method as an additional technique for stability are effective.

Keywords Earth retaining wall · Elasto-viscoplastic model · Excavation · Soft Holocene clay · Soil–water-coupled finite element analysis

✉ Fusao Oka
oka.fusao.38x@st.kyoto-u.ac.jp

Naoki Takada
takada-n@jrnc.co.jp

Kazuyuki Shimono
kazuyuki-shimono@westjr.co.jp

Yosuke Higo
higo.yohsuke.5z@kyoto-u.ac.jp

Sayuri Kimoto
kimoto.sayuri.6u@kyoto-u.ac.jp

[1] Lab. 3, Association for Disaster Prevention Research, Kyoto University, 138-1 Tanaka-Asukaicho, Sakyo-ku, Kyoto 606-8226, Japan

[2] JR West Japan Consulting, Co. Ltd., 5-4-20, Chuo Bldg., Yodogawa-ku, Osaka 532-0011, Japan

[3] Osaka Construction Office, JR West Japan, 5-4-20, Chuo Bldg., Yodogawa-ku, Osaka 532-0011, Japan

[4] Department of Urban Management Engineering, Kyoto University, C1 Bldg., Kyoutodaigaku-Katsura 4, Nishikyo-ku, Kyoto 615-8540, Japan

[5] Department of Civil and Earth Resources Engineering, Kyoto University, C1 Bldg., Kyoutodaigaku-Katsura 4, Nishikyo-ku, Kyoto 615-8540, Japan

1 Introduction

Many urban cities have been constructed over soft Holocene deposits with high ground water levels. It is known that, in the open-cut construction method, the ground and the retaining walls are often seen as being unstable if a complex construction process is not carefully followed. Many accidents during excavation works in such soft grounds have been reported (e.g., [19, 22]. In order to prevent the failure of the ground and to reduce the deformation of the ground during excavation works, a reliable prediction method and a high-level performance of the construction are required. For the last three decades, numerical methods have been used to predict the deformation and the failure of the ground and earth structures, such as retaining walls. Since the ground consists of sandy, clayey soils and the boundary conditions are generally complex, an appropriate modeling of the structure–ground system is needed. There are two methods for obtaining such a modeling. One is the imposed displacement method in which the displacement is calculated by the beam-spring model, using the subgrade reaction modulus, and then applied to the surrounding ground. The other is a method in

which the stress is released at the nodes of the finite element corresponding to the excavation of the soil. At present, the single-phase elastic finite element method is a useful method because it requires only a small number of parameters and is effective within the range of small strains, but not in the range of plasticity. And, it is known that the soil–water-coupled finite element method is a powerful tool for the analysis of the ground and soil structures. In practice, however, this method has not been popular at the design stage of projects (e.g., AIJ [1]. For cases in which the deformation gradients are small, the elastic method is applicable. However, for large-scale excavation problems in soft deposits with high water levels, the deformation is elasto-plastic or elasto-viscoplastic. Particularly for soft clay deposits, creep, as well as consolidation, may occur even though the creep is small. In the present paper, we used an elasto-viscoplastic model since experimental results show that the Osaka clay exhibits strain rate sensitivity as well as the fact that it is known the initial volumetric strain rate is not zero in soft clay layers caused by the self-weight. For the construction of the Osaka Station building, we conducted a soil–water-coupled elasto-viscoplastic finite element analysis during and after the excavation work to examine the construction method and to confirm the safety of the excavation work by comparing the measured and the simulated results. In the present paper, a numerical analysis of the excavation is presented and compared with the measured results. In the construction project, we used a deep mixing soil improvement method, called the "soil buttress method," as an additional technique for stability. In the analysis, we used a computer program, called COMVI2D-EX10 developed by Oka et al. at Kyoto University [13] and Boonlert et al. [2].

2 Geotechnical context at the excavation site

The construction was performed in the Umeda district, in the heart of the Osaka urban area. The soil profile in the Umeda district, shown in Fig. 1, is as follows: The surface fill layer comprises a heterogeneous mixture of sand, gravel, crushed stone, and construction material with a thickness of 2.5 m. Underlying the fill layer, there is an alluvial sandy layer (As) with a thickness of 2.5 m containing the fine content. Below the sandy layer (As), there is a soft alluvial clay layer (Ac) with a thickness of 20 m. The SPT values for the upper layer are 1–3, and they increase just around the bottom alluvial clay layer. At a depth of 16 m, the plasticity indices and the OCR of the alluvial clay layer are Ip = 24 and OCR = 1.55, respectively, while at a depth of 24 m, they are Ip = 47 and OCR = 1.56. The alluvial layers are underlain by a gravel layer (Dg1) which comprises gravel with particle sizes of 2–30 mm. The ground water of this Dg1 layer is artesian, and its SPT value is around 50. Below the Dg1 layer, there is a Pleistocene clay deposit (Dc) with a thickness of 10 m and an SPT value of 3–13. The Dc layer is underlain by a

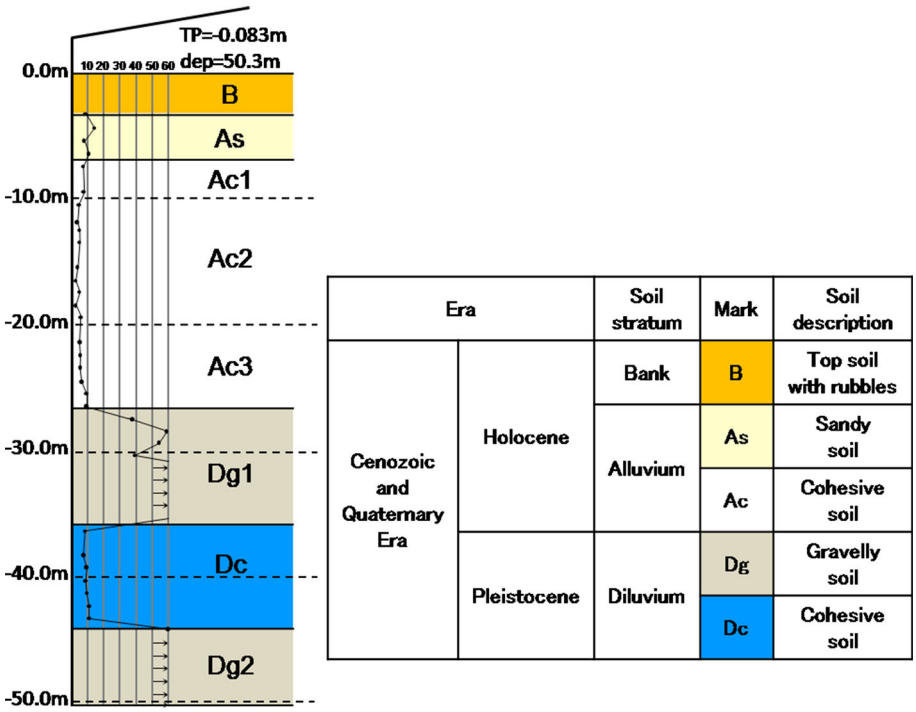

Era		Soil stratum	Mark	Soil description
Cenozoic and Quaternary Era	Holocene	Bank	B	Top soil with rubbles
		Alluvium	As	Sandy soil
			Ac	Cohesive soil
	Pleistocene	Diluvium	Dg	Gravelly soil
			Dc	Cohesive soil

Fig. 1 Soil profile

Holocene gravel layer (Dg2) that contains gravel with particle sizes of 2–30 mm. The SPT value is more than 50 and the ground water is artesian.

3 Representation of the excavation project

The JR West Japan Railway Company constructed a new building just at the north of the station as part of a reconstruction project of Osaka Umeda Station (JR West Japan Railway Company [18, 21]. The construction started in April of 2007 and ended in May of 2010. This construction was performed just beside an existing railway line. Figure 2 shows a plane view of the excavation works in which the excavation area is surrounded by red and blue solid lines. The nearest point along one of the retaining walls is 1.3 m from the piers supporting the existing elevated railway tracks. The depth of the excavation is 20 m, the width of the cross section is 29–62 m, and the length is 252 m, as shown in Fig. 2.

In this construction, the excavation was performed inside the surrounding earth retaining walls. A plane strain two-dimensional analysis is preferable due to its shorter computation time. According to Finno's study [5], when the ratio of the length of the excavation over the width is more than 2.0 and the ratio of the length over the depth is more than 6.0, the results of a three-dimensional analysis and a two-dimensional plane strain method will be similar. In the present case, the length of the excavation (L) is 165–252 m, the width (B) is 29–62 m, and the depth (H) is 19.66 m, indicating that the analysis under plane strain conditions would yield similar results to the three-dimensional analysis, since $L/HE = 8.4$–12.8 and $L/B = 2.7$–8.7.

The construction of the retaining walls and the excavation may be described as follows. The retaining wall beside the existing elevated piers is an RC diaphragm wall with high rigidity to prevent deformation. It has a thickness of 1.2 m, a length of 44 m, and it is used as the main structure of the building. The other retaining wall is a trench cutting re-mixing deep wall (TRD); it can maintain continuity in the direction of the retaining wall. The excavation technique is the inverted lining method applied to effectively reduce settlement and leaning; the excavation is performed downward (top to bottom) by strutting the retaining wall.

4 Soil improvement technique

The buttress type of deep mixing method was used to reduce the displacement of the retaining wall beside the railway structures in which the ground is partially improved [4]. This method is economical and less time-consuming than the method in which the entire ground is improved. The allowable displacement limits for the safety of trains is 15 mm for both vertical and horizontal track deviations. The relative displacement limit between piers for the elevated tracks is 10 mm (secondary allowable action limit) considering the results from an analysis of elastic frames. The specifications for the improved ground are determined as follows.

The mixing diameter of one circular column is 0.9 m, and its equivalent effective width is 0.8 m, which is equivalent to the square column shown in Fig. 3. The installation interval is 4.5 m, the improved length is 7.2–20.4 m, and the installation depth is GL-0.0 to 28 m,

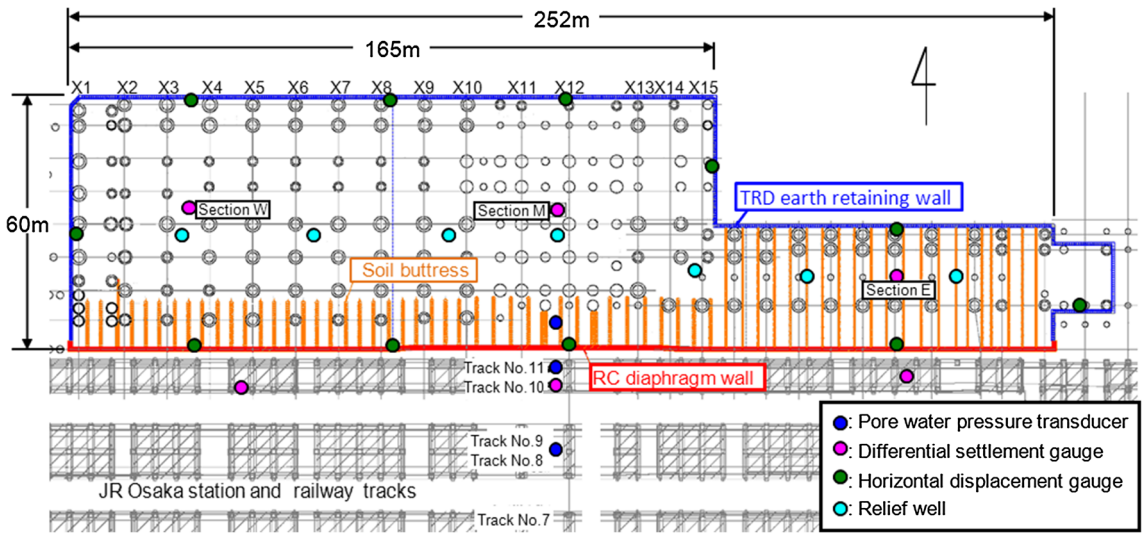

Fig. 2 Plane view and the measuring points

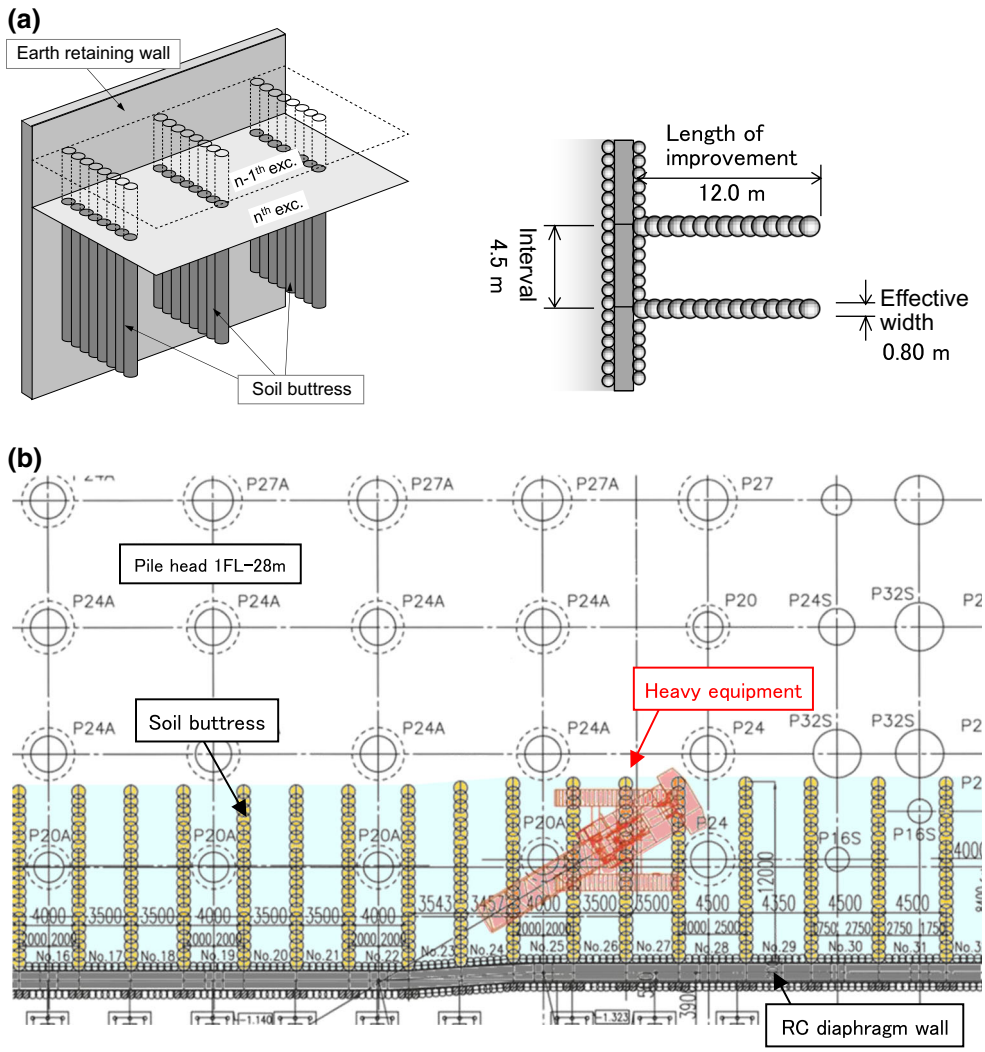

Fig. 3 **a** Schematic figure of ground improvement method. **b** Plane view of ground improvement

which was determined by considering the trafficability and economical conditions. A schematic figure of the buttress type of deep mixing is shown in Fig. 3a, while a plane view is given in Fig. 3b.

4.1 Excavation process

The excavation area is divided into three parts from the west side, namely, W area, M area, and E area, as shown in Fig. 2; an excavation was carried out in each area. The inverted lining method was used for the excavation to prevent deformation; six bench beams (struts used in the step-by-step excavation) and seven bench excavations, as shown in Fig. 4, were employed. After the second, fourth and sixth excavation procedures, preloads (50 %) were installed for the oblique beams to prevent deformation. The construction procedure (Steps 1–13) for the central part of the cross-sectional excavation at M area in Fig. 2 is shown in Fig. 5. Construction area *M* consists of four areas at each step, as shown in Fig. 6. After the second excavation procedure, the other procedures were conducted starting from the area farthest from the existing pier used to support the elevated tracks as MA → MB → MC → MD, shown in Figs. 5 and 6.

4.2 Ground water level

A relief well was installed at the center of the excavation area to lower the water level of the pressurized Pleistocene gravel layer, Dg1. To reduce the heaving of the ground during excavation procedures, it is common to use a relief well to decrease the water level. The analysis took account of the changes in water level of Dg1 through the relief well, as shown in Fig. 9.

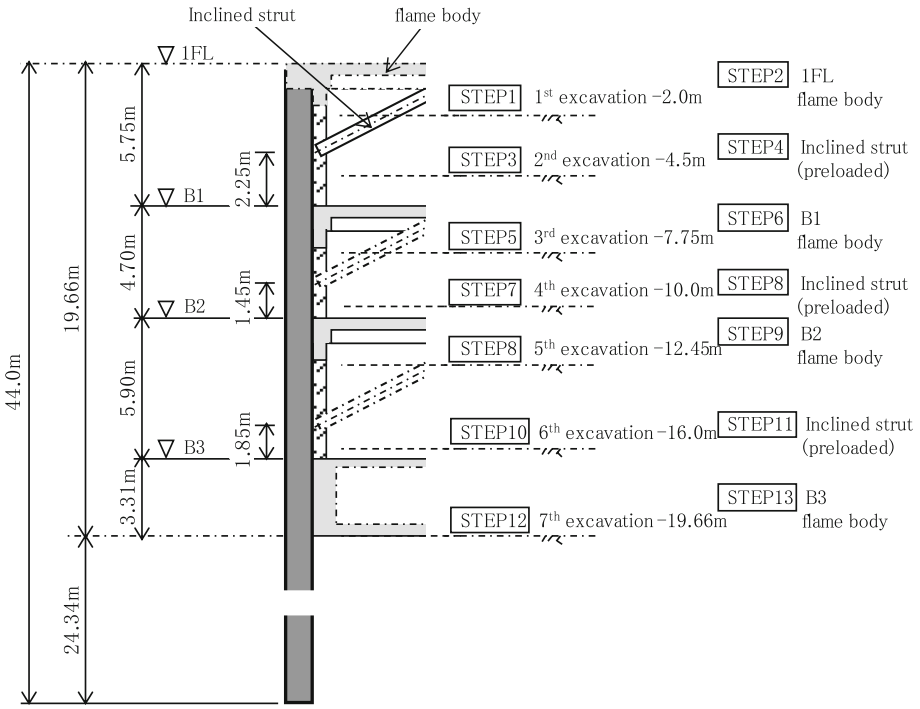

Fig. 4 Excavation procedure

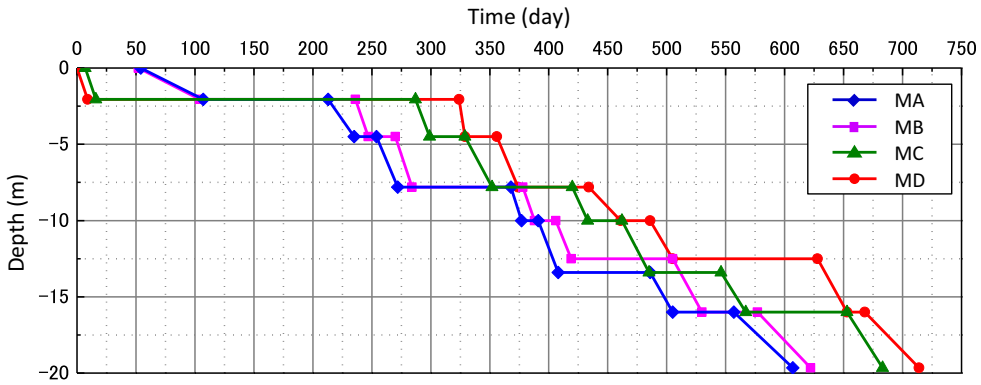

Fig. 5 Construction time history at sections

5 Numerical calculation

5.1 Elasto-viscoplastic constitutive equation

The constitutive model for clay is an over-stress type of elasto-viscoplastic model by Kimoto and Oka [10], which can describe the degradation induced by strain, such as strain-softening behavior. An outline of the model is given in Appendix 1.

The model has been applied to several problems such as the consolidation of a soft foundation [9] and an excavation [14]. The model parameters for the clay layers used in this analysis were determined through undrained triaxial compression tests with different strain rates and through consolidation tests to clarify the viscoplastic rate effect.

5.2 Determination of material parameters used in the analysis

For the material parameters, we have used the experimental results for clay layers and the empirical relations for sandy and gravel layers, such as As, Dg1, and Dg2, partly considering the measurement results for the permeability. In order to clarify the mechanical characteristics of Osaka Umeda clay and its material parameters for the elasto-viscoplastic model, undrained triaxial tests and model simulations were performed using an elasto-viscoplastic

model by Kimoto and Oka [10]. Undrained triaxial compression tests have been carried out for the soil specimens taken from the Ac2 layer at a depth of GL-16.0 m and from the Ac3 layer at a depth of GL-21.0 m; the results are shown in Fig. 7. The undrained triaxial compression tests were conducted with different axial strain rates, namely, 0.005 and 0.05 % min, to obtain viscoplastic parameter m' for the specimen sampled at a depth of GL-21.0 m. The viscoplastic parameters of Ac1 layer have been determined by the triaxial tests.

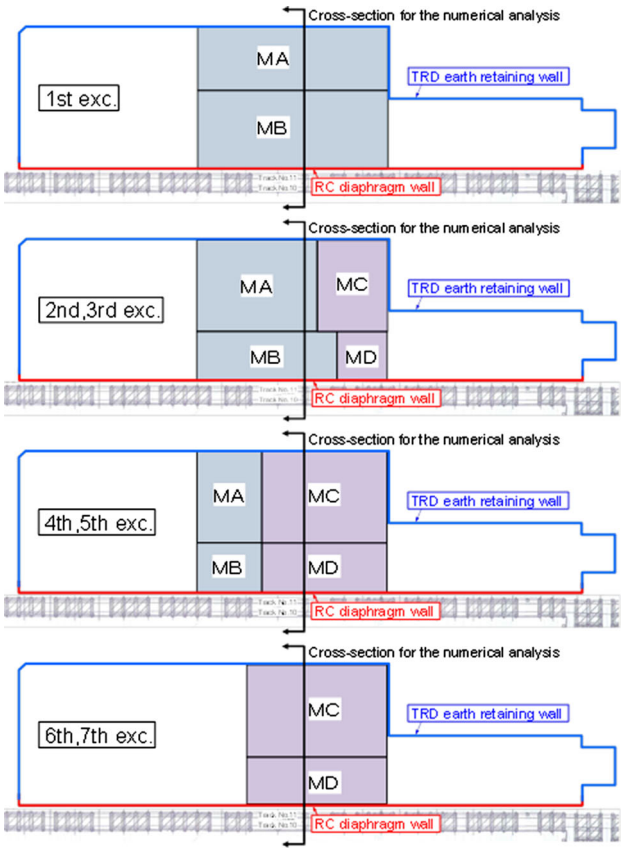

Fig. 6 Division of *M* area and the study section

The material parameters used in the simulation of soft clay are listed in Table 1. The method of parameter determination is shown by Kimoto and Oka [10] and Oka and Kimoto [15]. Compression index λ, swelling index κ, and consolidation yield stress (conventionally called preconsolidation pressure) σ'_{mbi} were determined by consolidation tests. Initial elastic shear modulus (tangential modulus at zero strain) $G0$ was determined by adjusting it to the test results. Viscoplastic parameter m' is a parameter that exhibits the strain rate effect. The value of the parameter is similar to the value of the Osaka soft clay in the Nakanoshima district of Osaka City [12, 14].

Viscoplastic parameters C_{01} and C_{02} can be determined by the initial values of the strain rates, i.e., initial volumetric and deviatoric strain rates, but it is not such an easy task. Hence, we can determine these values from the overall behavior of the soil. For parameters C_{01} and C_{02}, we firstly assumed that $C_{01} = C_{02}$. Then, if the dilatancy effect is not appropriately simulated, we change C_{02} to more accurately reproduce the stress path or the volumetric strain. Structural degradation parameter σ'_{maf} was determined by the difference between the peak stress and the stress at a large strain. The other structural parameter, β, was determined considering the rate of strain softening. The simulated and the experimental results are shown in Fig. 7, which indicates that strain rate sensitivity and strain-softening behaviors are reproduced in both the stress paths and the stress–strain relations. The elastic shear modulus is determined by the stress–strain relation and consolidation tests for the clayey layers, while the permeability coefficients are determined by in situ lifting pumping tests for the sandy layers and by multi-phase consolidation tests for the clayey layers. For the elastic modulus, we used Young's modulus, which is a smaller value than the initial tangential one, to take account of the

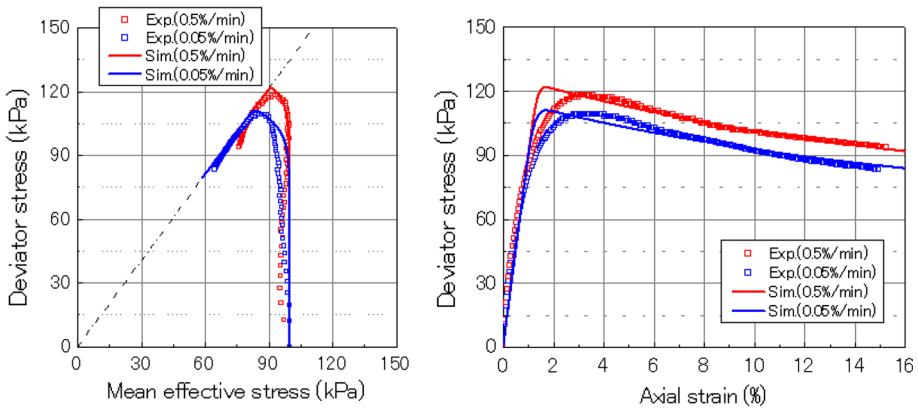

Fig. 7 Simulation of undrained triaxial compression tests and experimental results

Table 1 Material parameters used in simulation

		Ac2 (GL-16.0 m)	Ac3 (GL-21.0 m)
Initial elastic shear modulus (kPa)	G_0	3000	3000
Compression index	1	0.295	0.314
Swelling index	K	0.0384	0.0369
Initial void ratio	e0	1.26	1.37
Stress ratio at failure	M_f^*	1.102	1.070
Viscoplastic parameter	m'	20.38	12.22
Viscoplastic parameter (1/s)	C_{01}	4.0×10^{-9}	1.5×10^{-7}
Viscoplastic parameter (1/s)	C_{02}	3.0×10^{-8}	1.0×10^{-7}
Initial mean effective stress (kPa)	σ'_{mo}	100	130
Consolidation yield stress (kPa)	σ'_{mbi}	172	292
Structural parameter (kPa)	σ'_{maf}	90	130
Structural parameter	β	5.0	5.0

strain dependency considering the overall curve fitting. It is known that viscoplastic parameters C_{01} and C_{02}, determined by laboratory tests, e.g., C_{02}, is related to the initial strain rates might be larger than those under in situ conditions because the strain rates after consolidation in the laboratory are larger than those under in situ conditions possibly caused by the disturbance, eg., indicated by Leroueil et al. [11]. And the viscoplastic parameters C_{01} and C_{02} are inversely proportional to the consolidation yield stress which depends on the strain rate (Oka and Kimoto [15]). Considering the previous application of the model to Osaka clay [14], C_{01} and C_{02} are assumed to be 10^{-2} times smaller for Ac2 and 10^{-3} times smaller for Ac3. When we use smaller values for C_{01} and C_{02}, the peak values for the deviator stress are about 25 % higher than those by the values on Table 1. Figure 7 indicates that the behavior is pseudo-elastic before peak stress, but the viscoplastic strain is not zero. It is worth noting the strain level of the ground is not so high in the whole domain, but may be high locally, e.g., near the excavation front. In addition, the strain at the peak stress obtained in the triaxial test probably is larger than that under in situ conditions because of the sample disturbance.

For the shear elastic modulus $G0$, we used the larger value of Table 3 in the FE analysis than that of Table 1 due to the same reason of the sample disturbance induced by the sampling process.

For the soils without experimental or measured values, such as the As (alluvial sand), Dg1 (Pleistocene gravel) and Dg2 (Pleistocene gravel) layers, we estimated the elastic coefficients and Young's modulus E, which is not a secant modulus, but includes some strain dependency based on the empirical formula using the SPT N value by Railway Technical Research Institute of Japan (RTRI), which was first proposed by Uto [20]. RTRI [16] proposed several methods to determine Young's modulus including the shear wave velocity. However, we have adopted a method using the SPT N value because of the limited data as

$$E = 2500\,\mathrm{N} \quad (\mathrm{kN/m^2}), \quad N: \text{ SPT value} \tag{1}$$

This formula has been successfully used in the design of railway-related architectural structures for many years confirming the agreement with the measured results (RTRI 16).

Poisson's ratio v is given by the formula as

$$v = K_0/(1 + K_0), \tag{2}$$

where K_0 is the earth pressure coefficient at rest to be obtained by Jaky's formula. In the calculation, RTRI [16] proposed the correction of Young's modulus estimated by Eq. (1) based on the measurement of rebound for the excavation. RTRI [16] recommends that a 2- to 3-times larger Young's modulus is appropriate when analyzing the rebounding induced by the relatively large excavation in the construction works. Poisson's ratio for the As, Dg1, and Dg2 layers has been estimated considering Eq. (2) because we did not have enough experimental data for these layers.

For the other parameters for As and Dg layers, we used parameters obtained for the same layers at Nakanoshima near Umeda in Osaka which were reported by Oka et al. [14]. due to the lack of experimental data.

The soil improved by deep mixing for the soil buttress is assumed to be elastic, and the material parameters for the soil buttress–soft soil composite material were determined by weighing the elastic constants of the soil buttress and the soft soil between the soil buttresses with respect to the widths of the materials for the interval of the installation (about 4.5 m). The composite material is assumed because of the two-dimensional modeling. The setting of the soil improvement (soil buttress) is shown in Fig. 3a; the interval of the soil buttress = 4.5 m, the length of the soil

buttress = 7.2–20.4 m, and the effective width of soil buttress = 0.8 m.

The material parameters used in the analysis are listed on Table 2. In the finite element analysis, the sandy soil is modeled as a linear elastic model because not enough data existed and large deformation is not expected. The soil buttress body is also modeled as linear elastic materials. The Young's modulus of the soil buttress is determined by one-dimensional compression test results, and its permeability coefficient and Poisson's ratio are determined by the value recommended by the Japan Architecture Center [8]. The RC continuous wall is modeled as a linear elastic material, and the strut beam is a linear elastic spring (RTRI [17]. The permeability of the RC continuous wall was determined as 1.0×10^{-10} (m/s) based on the records of the measured data.

Table 2 Parameter used in analysis

	Acl	Ac2	Ac3	Dc	
(a) Elasto-viscoplastic parameters for soft soil					
Unit weight (kN/m3)	γ	16.5	16.5	16.6	16.8
Initial elastic shear modulus (kPa)	$G0$	9700	14,750	17,600	30,100
Permeability coefficient (m/s)	k	2.11×10^{-9}	1.08×10^{-9}	5.92×10^{-10}	3.46×10^{-10}
Compression index	λ	0.236	0.295	0.314	0.402
Swelling index	K	0.0298	0.0384	0.0369	0.0400
Initial void ratio	$e0$	1.43	1.26	1.37	1.50
Over-consolidation ratio	OCR	1.52	1.72	2.25	2.49
Stress ratio at failure	M_f^*	0.972	1.102	1.070	0.776
Viscoplastic parameter	m'	20.38	20.38	12.22	27.59
Viscoplastic parameter (1/s)	C_{01}	4.0×10^{-11}	4.0×10^{-11}	1.5×10^{-10}	2.0×10^{-14}
Viscoplastic parameter (1/s)	C_{02}	3.0×10^{-10}	3.0×10^{-10}	1.0×10^{-10}	2.0×10^{-13}
Structural parameter (kPa)	σ'_{mb}	$\sigma'_{mo} \times$ OCR	$\sigma'_{mo} \times$ OCR	$\sigma'_{mo} \times$ OCR	$\sigma'_{mo} \times$ OCR
Structural parameter	β	5.0	5.0	5.0	15.0

		B	*As*	*Dgl*	*Dg2*
(b) Elastic parameters for soils					
Unit weight (kN/m3)	γ	18.0	18.0	20.0	16.3
Young's modulus (kPa)	E	7000	8400	225,000	450,000
Poisson's ratio	v	0.32	0.32	0.27	0.28
Permeability coefficient (m/s)	k	5.50×10^{-5}	5.50×10^{-5}	3.10×10^{-3}	4.54×10^{-6}

		Diaphragm wall	Composite ground with soil buttress				
			B-As	Ac1	Ac2	Ac3	Dg1
(c) Material parameters for improved soil (elastic material)							
Unit weight (kN/m3)	γ	24.5	–	–	–	–	–
Young's modulus (kPa)	E	$2.65 \times 10'$	34,600	57,300	59,300	55,000	263,000
Poisson's ratio	v	0.20	0.311	0.364	0.388	0.324	0.271
Permeability coefficient (m/s)	k	1.0×10^{-10}	4.40×10^{-5}	1.71×10^{-7}	8.87×10^{-8}	4.94×10^{-8}	2.44×10^{-3}

Strut	Type of supports	Specifications	Spring constant KH (kN/m2)
(d) Parameters for support structures (elastic material)			
First strut	Slab	$t = 250$ mm	197,000
Second strut	Inclined strut, slab	H-400, $t = 250$ mm	59,000
Third strut	Slab	t = 250 mm	118,000
Fourth strut	Inclined strut, slab	H-400, $t = 150$ mm	50,000
Fifth strut	Slab	$t = 150$ mm	118,000
Sixth strut	Inclined strut, slab	H-400, $t = 150$ mm	50,000

H-400: strut (H-section steel beam), (Height = 400 mm, $B = 400$ mm), t thickness of slab

6 Numerical modeling

For the numerical simulation, we used a finite element method for two-phase mixtures based on the finite deformation theory. The governing equations and the analysis method are described in Appendix 2. The mesh for the analysis comprises 2530 elements and 7793 degrees of freedom. For the solid skeleton, we used eight-node isoparametric elements for the solid skeleton and four-node isoparametric elements for the pore water pressure.

6.1 Modeling of the excavation process

The excavation procedure used in this analysis was based on the method by Brown and Booker [3]. The equivalent stress due to the excavation was calculated from the excavated elements adjacent to the excavation boundary using the following equation:

$$\{\boldsymbol{R}_E\} = \int_{V_E} [\boldsymbol{B}]^{\mathrm{T}}\{\sigma\}\mathrm{d}v - \int_{V_E} [\boldsymbol{N}]^{\mathrm{T}}\rho\{b\}\mathrm{d}v \tag{3}$$

in which $\{\boldsymbol{R}_E\}$ is the force vector appropriate to the nodes on the excavated surface, $[\boldsymbol{N}]$ is a matrix for the shape function of the eight-node isoparametric element, $[\boldsymbol{B}]$ is the strain–displacement matrix, $\{\sigma\}$ is the total stress vector in the elements to be excavated, ρ is the wet density, $\{b\} = \{0, g\}$ is the body force vector, g is the gravitational force, and V_E is the volume of the excavated element. The excavation process was incrementally analyzed. The finite elements, boundary conditions, and cross section of the analysis are shown in Fig. 8.

The areas are divided into small sections at each excavation stage for the excavation shown in Fig. 6. In the analysis, we have adopted the two-dimensional analysis method under plane strain conditions for a cross section. Half of the cross section of the excavation area has been calculated according to the computation time, namely, from the diaphragm wall to the center of the excavation area. Hence, the excavation procedures for sections MB and MD of the construction area in Fig. 4 have been taken in the analysis. Figure 9 indicates the construction–time profile for sections MB and MD.

For the relief well, shown in Fig. 8, the water head boundary has been employed. The prescribed pore water pressure, corresponding to the water head of the relief well installed in stratum Dg1 (Figs. 8 and 9), was given to the boundary.

6.2 Initial stress

For the initial stress calculation, we only considered the dead load of 80 kN/m2 induced by the existing pier supporting the elevated tracks as well as the self-weight. In addition, other loads induced by various activities such as such as railway trains, cars, and a crowd of people at the station were applied to the surface as 10 kN/m2 .

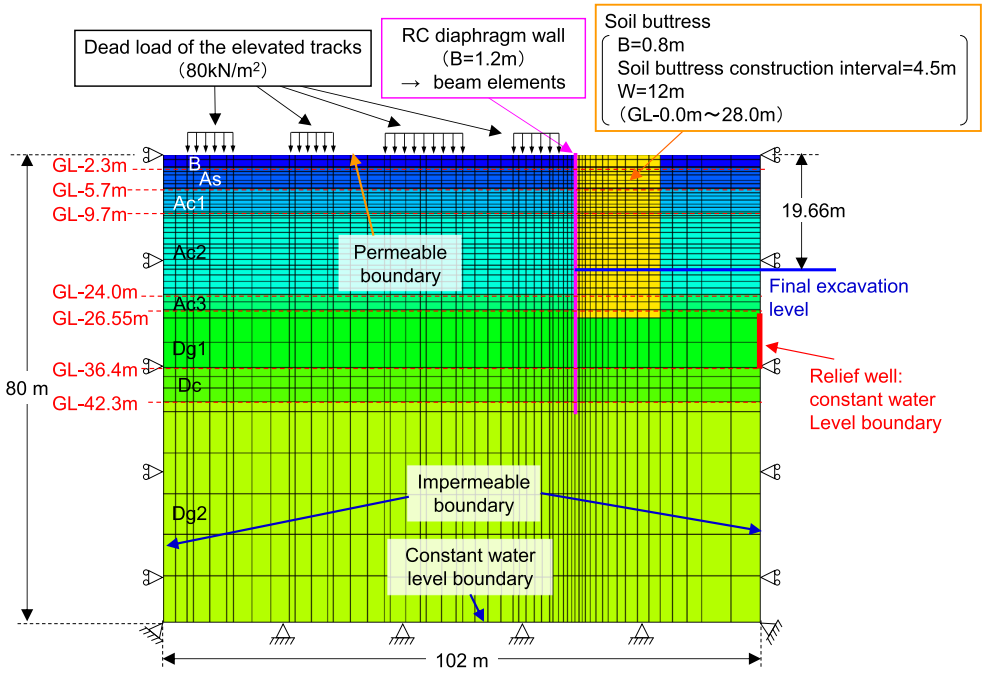

Fig. 8 FEM mesh and boundary conditions

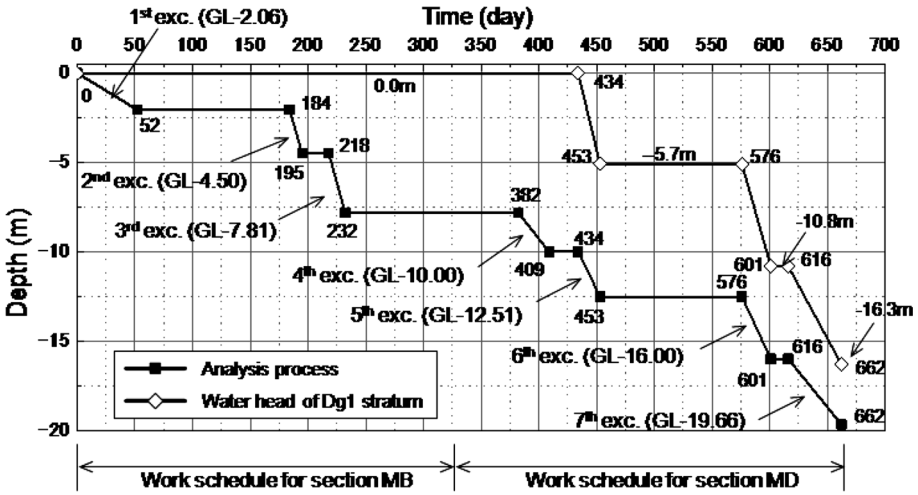

Fig. 9 Construction–time profile

Table 3 Preloads of strut beam

Strut	Type of supports	Specifications	Preload (kN/m)
First strut	Slab	$t = 250$ mm	0.0
Second strut	Inclined strut, slab	H-400, $t = 250$ mm	96.0
Third strut	Slab	$t = 250$ mm	0.0
Fourth strut	Inclined strut, slab	H-400, $t = 150$ mm	117.0
Fifth strut	Slab	$t = 150$ mm	0.0
Sixth strut	Inclined strut, slab	H-400, $t = 150$ mm	106.0

H-400: strut (H-section steel beam), (Height = 400 mm, $B = 400$ mm), t thickness of slab

7 Results and comparisons with measurements discussions

7.1 Comparison of measured and simulated results

7.1.1 Displacement of earth retaining wall

The preloads of the strut beam are listed in Table 3. The distribution of the measured and the simulated horizontal displacements of the retaining wall is shown in Fig. 10. In general practice, it is often assumed that the deepest point of the retaining wall is a fixed point, but in the Osaka soft clay deposit, it has been reported that the deepest point of the wall, which penetrates into the diluvial gravel layer, displaces even in the deep diluvial gravel layer in the case of large-scale excavations [14]. For this reason, we have measured the top of the wall with respect to the fixed zero displacement point, and then inversely calculated the displacement of the deepest point of the wall. The displacement into the excavation area is positive. It is seen that the excavation induced the wall to move into the excavation area and that the value is 14.0 mm 751 days after the beginning of the excavation and 89 days after the end of the excavation.

Figure 10a, b shows that the trends of the displacement developments of the retaining wall agree with those of the measured ones. Until the third stage of the excavation, the simulated displacement is larger than that of the measured one, namely, by 10 mm. This may be due to the setup of the initial stress levels. The initial value is not zero because the other areas, such as MC and MD, had been started before that of MB, as shown in Fig. 6. In order to fully take into account the effect of the all the other areas, a three-dimensional analysis is required.

Supplemental data Fig. 11 show the time history of the horizontal displacements of the retaining wall. Although the excavation was not performed from day 52 to day 161, the deformation continued. This is partly due to the viscoplastic creep and consolidation phenomena of the clay layer; the present analysis can reproduce the behavior of the retaining wall from day 52 to day 161, although the value is rather small.

7.1.2 Settlements in layers

The installation points of the settlement gauges are indicated in Fig. 12. Figure 13a, b shows the vertical displacement–time profile at depths of GL-2.5 m and GL-

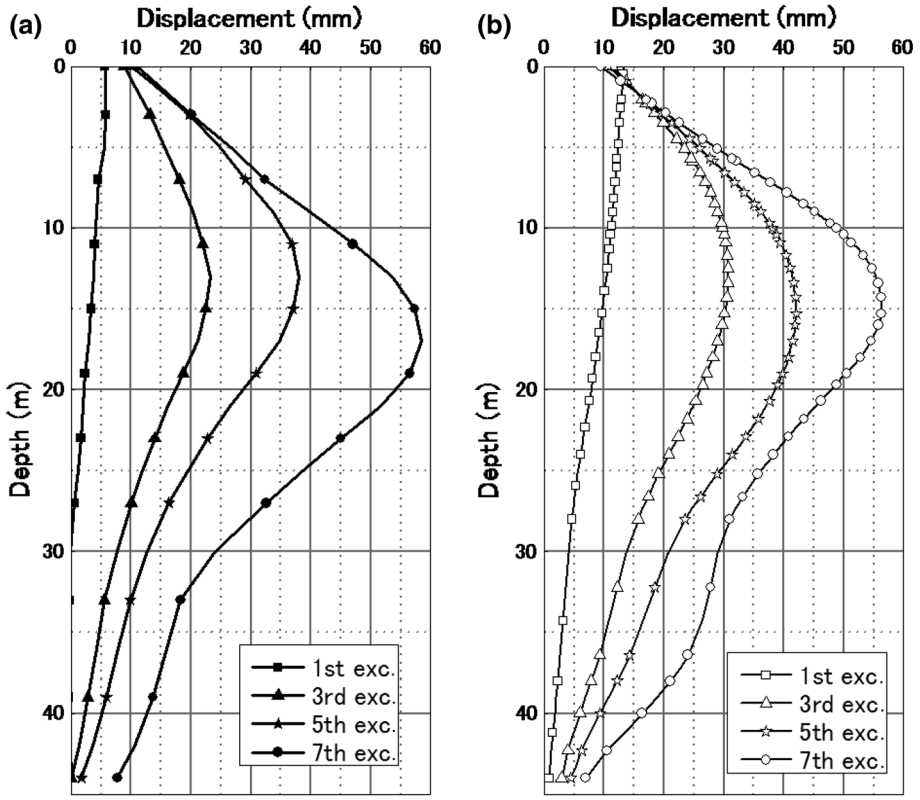

Fig. 10 **a** Displacement profile of retaining wall (observed). **b** Displacement profile of retaining wall (simulated)

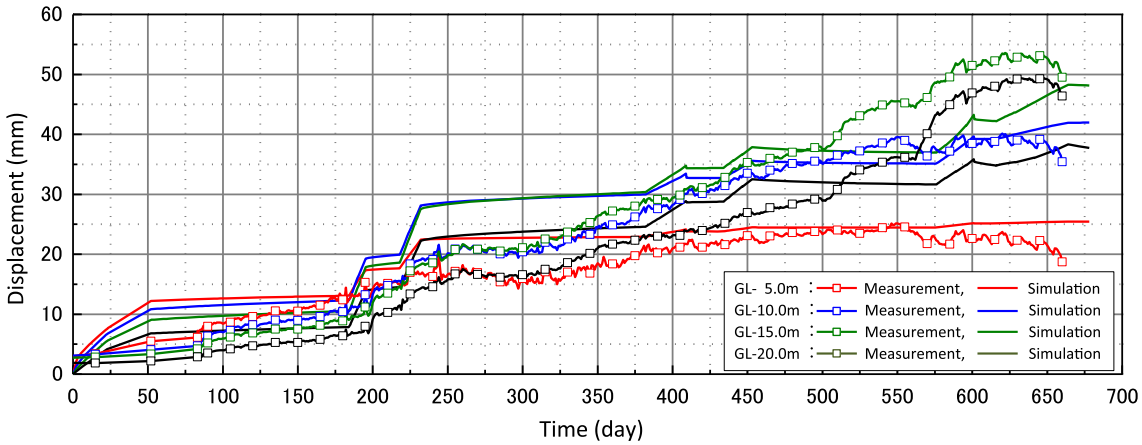

Fig. 11 Displacement of the retaining wall–time profile

7.5 m behind the retaining wall, respectively. Looking at Fig. 13a, the simulated results correspond to the 1st stage of the excavation until day 52. In this period, the simulated settlement is rather larger. This may be due to the underestimation of the elastic modulus.

Between days 52 and 184, the excavation was stopped; during this period, a settlement of almost zero was observed. Between days 184 and 232, i.e., during the second and third stages of the excavation, the settlement developed and corresponded to the measured results. From days 232–382, the excavation was stopped again; the simulated settlement was almost zero and a small settlement was seen in the measurement. This observed settlement may be due to the excavation at the other sections, MC and MD. This point is partly due to the assumption of two-dimensional analysis of the three-dimensional real behavior. Between days 382 and 453, i.e., during the fourth and fifth stages of the excavation, the simulated settlement is similar to the measured value. Then, the excavation was stopped again between days 453 and 576. In this period, the

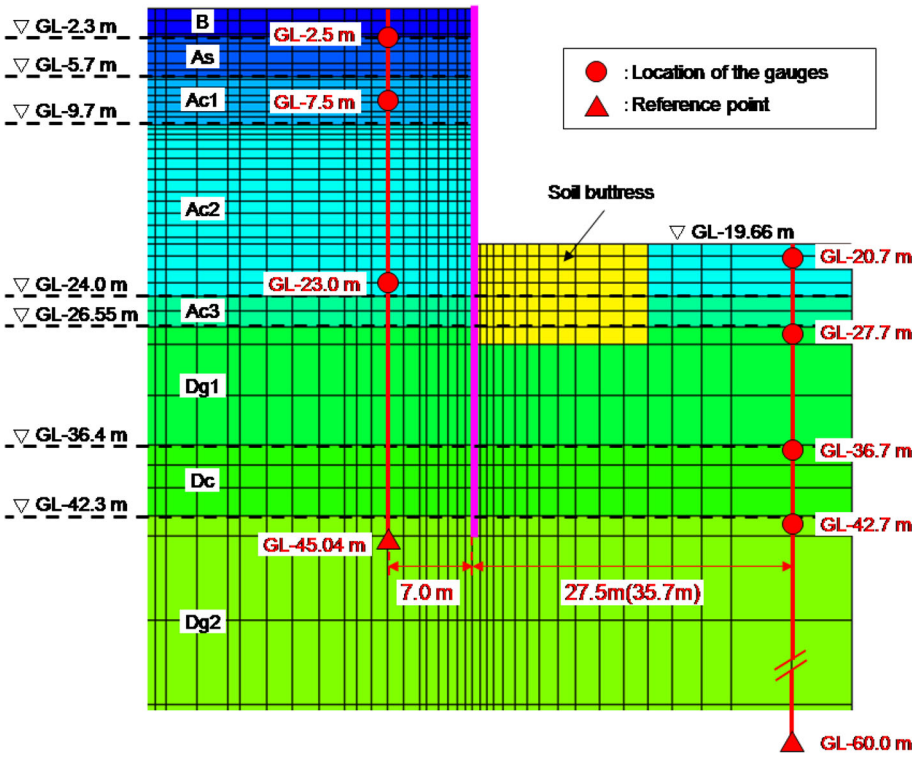

Fig. 12 Location of settlement gauges

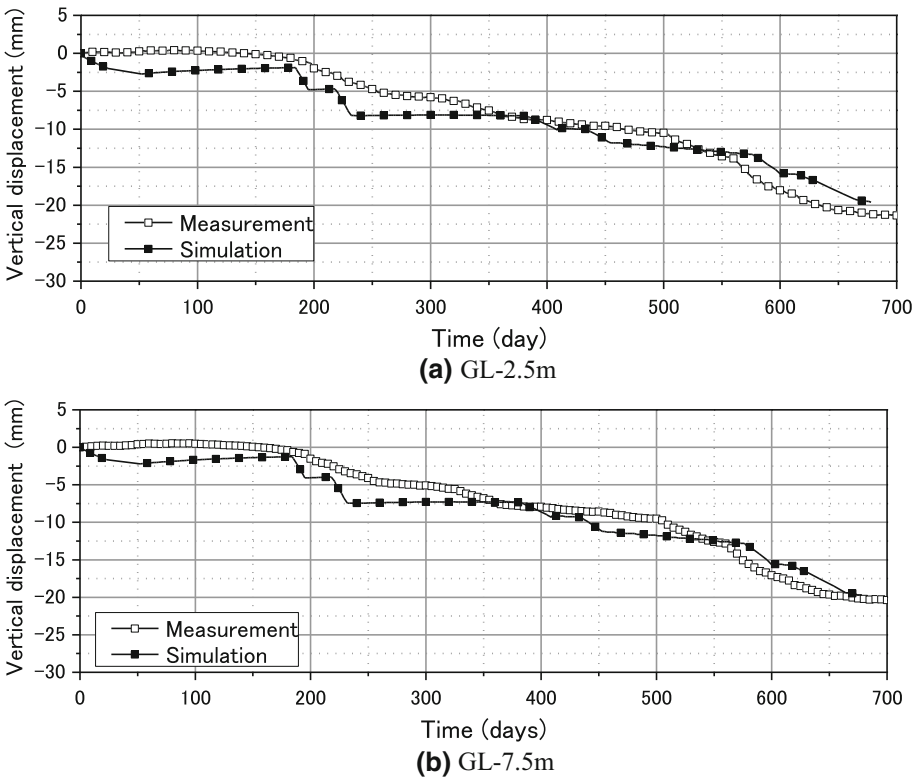

Fig. 13 Vertical settlement–time relation at a depth of GL-2.5 (**a**), -7.5 m (**b**) behind the retaining wall

settlement still developed, although the magnitude was small. This is probably due to viscoplastic creep and/or consolidation.

Figure 14 shows the simulated pore pressure–time profile during the excavation. The pore water pressure increases, e.g., between days 232 and 382 in Fig. 14, while the settlement is almost zero during the period in Fig. 13. This phenomenon can be explained as follows; the pore water pressure develops due to the development of the viscoplastic volumetric strain during this period, but the dissipation of the pore pressure is not enough for the settlement of the ground. This is a feature of the consolidation of the viscoplastic ground. Then, the pore water pressure gradually decreased with time. This indicates the progress of the consolidation of the clay layer.

Finally, settlement occurred during the sixth and seventh excavation periods, i.e., between days 576 and 662. The increase in displacement just after the excavation is consistent with the displacement of the retaining wall shown in Fig. 8. The settlement–time profile at a depth of 7.5 m is similar to that at a depth of 2.5 m. The overall trend of the simulated and observed settlement–time profiles at depths of 2.5 and 7.5 m are in good agreement, except for the settlement behavior at the shallow depth in the very early stages of the excavation.

In Fig. 15, the vertical settlement–time relations in the excavation area at a depth of 20.7 m are shown. Both the measured settlement and the simulated results exhibit a

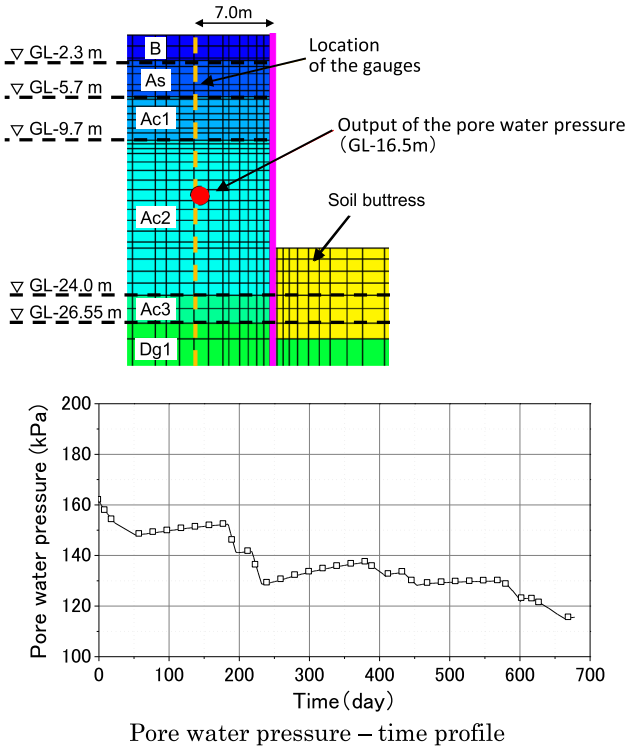

Fig. 14 Pore water pressure–time profile

rebounding trend. We can see that the simulated results are consistent with the measured results until day 200. After day 200, however, the simulated results are larger than the measured ones. This is partly due to the inverted construction method of the lining and the simultaneous construction of the piles. The distribution of the simulated viscoplastic volumetric strains at the end of the excavation is shown in Fig. 16a, b, which indicates that expansive strain occurs in the Ac3 and Dc layers and that the viscoplastic volumetric strain is compressive in the Ac1 and Ac2 layers. This denotes that the rebounding is due to the elastic deformation. One of the reasons for the limited rebound in the measured results is the constraint brought about by the installation of the building piles; another reason is the over-estimation of the rebound in the analysis due to the smaller elastic constants assumed in the model. From these results, it is seen that the elastic modulus has to be determined more accurately and that it is necessary to include the construction procedure in more detail.

Next, we will discuss the degradation of the ground through the estimation of the distribution of accumulated viscoplastic deviatoric strain γ^{VP} which is defined as

$$\gamma^{\mathrm{VP}} = \int \mathrm{d}\gamma^{\mathrm{VP}}, \quad \mathrm{d}\gamma^{\mathrm{VP}} = \left(\mathrm{de}_{ij}^{\mathrm{VP}}\mathrm{de}_{ij}^{\mathrm{VP}}\right)^{\frac{1}{2}}, \quad \mathrm{de}_{ij}^{\mathrm{VP}} = \mathrm{d}\varepsilon_{ij}^{\mathrm{VP}} - \frac{1}{3}\delta_{ij}\mathrm{d}\varepsilon_{\mathrm{kk}}^{\mathrm{VP}} \tag{4}$$

in which $\mathrm{d}\varepsilon_{ij}^{\mathrm{VP}}$ is the viscoplastic strain increment tensor and δij is Kronecker's delta. γ^{VP} is a parameter that reflects the degradation of the ground.

Looking at the distribution of the accumulated viscoplastic deviatoric strain at the end of the excavation in Fig. 17, it is seen that γ^{VP} is larger in front of the improved ground around the center of the excavated area. The maximum value for γ^{VP} is 2.4 % behind the retaining wall and in the excavation area at the final excavation stage. This is consistent with the simulation results which show that the creep and consolidation effects become large after the end of the fourth excavation stage. Strain occurs just around the retaining wall. In the other areas, the strain is relatively small, such as less than 0.3 %. Strain of less than 0.3 % denotes that the stress level of the ground is much less than the strain at the peak stress observed in the triaxial tests; this indicates that the developed strain is smaller. This means the excavation works have been performed safely.

8 Conclusions

A numerical simulation of a deep excavation through a thick soft clay deposit using a soil–water-coupled finite element method with an elasto-viscoplastic constitutive model has been carried out. The material parameters were

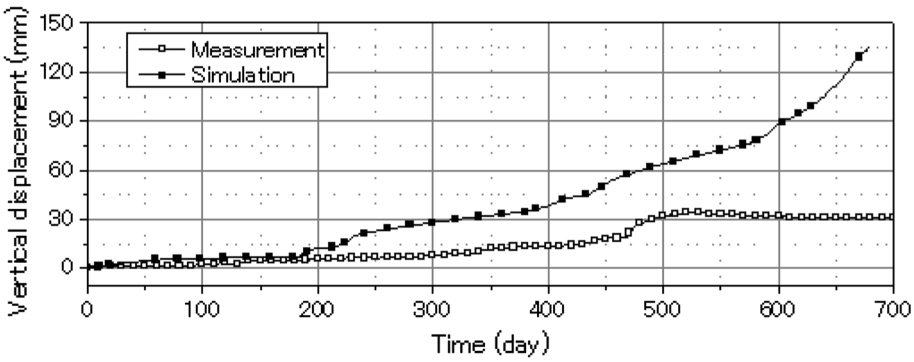

Fig. 15 Vertical settlement–time relation at a depth of GL-20.7 m in the excavation area

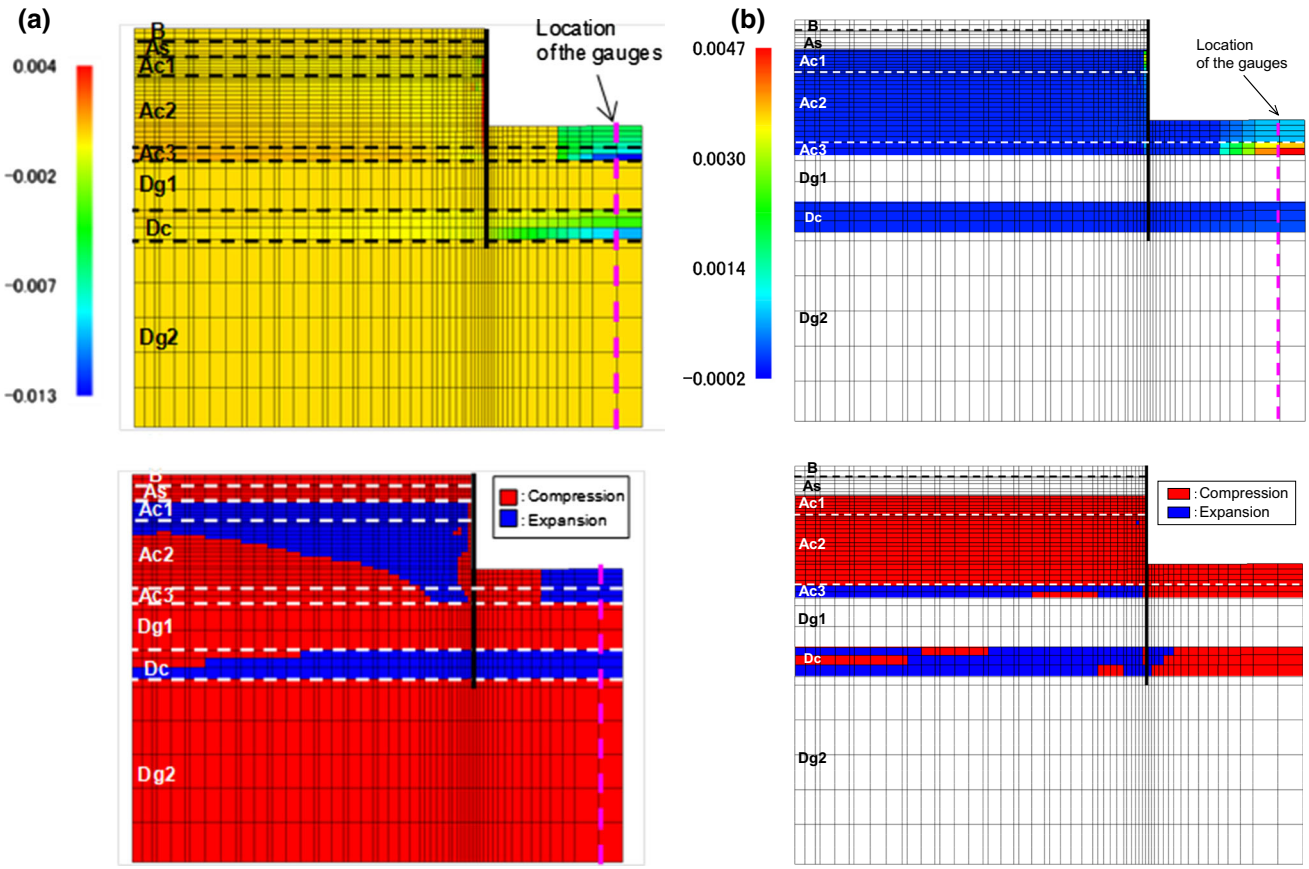

Fig. 16 **a** Distribution of elastic volumetric strain at the final stage of the excavation. **b** Distribution of viscoplastic volumetric strain at the final stage of the excavation

determined by the undrained triaxial tests for soft clay layers and the empirical law for the sand and the Pleistocene layers due to the limited information. The following conclusions have been obtained through the simulation of the large-scale excavation works in a construction area related to the renewal of the JR West Osaka Station.

1. The simulated deformation of the retaining wall was found to be in relatively good agreement with the overall measured results, but larger than the measured one. The large displacement in the excavation area is partly due to the building piles used in the construction and partly to an underestimation of the elastic modulus. In addition, it was found that the bottom of the retaining wall moved toward the excavation area.
2. The settlement behavior of the ground behind the wall has been well simulated. However, the progress of the deformation, even during periods of time when the

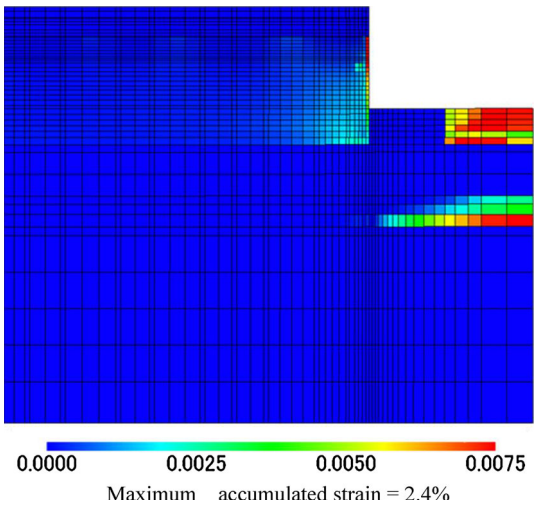

Fig. 17 Distribution of accumulated viscoplastic deviatoric strain at the end of excavation

excavation was stopped, indicated the possible effects of viscoplastic creep and associated consolidation. The simulated pore water pressure–time profiles partially showed viscoplastic deformation during the progress of the excavation in the simulation.

3. The accumulated viscoplastic deviatoric strain at the end of the construction was found to be larger around the retaining wall, as well as in the excavated area, for both Ac and Dc layers.
4. The rebound behavior in the excavation area was simulated, but the simulated rebound value was larger. This indicates that the complexity of the construction procedure affected the results and that the estimation of the elastic modulus is of great importance.
5. The buttress type of deep mixing method was found to be effective for reducing the deformation even when the improvement area was limited.
6. Comparing the measurement and the simulation results, it has been shown that the numerical simulation method reproduces the overall behavior of earth retaining walls relatively well only if the displacement at the bottom of the walls is taken into account. However, more consideration must be given to the construction procedure, and an accurate determination of the parameters is required in order to more accurately simulate all of the measurements. This is because the small accumulation of viscoplastic deviatoric strain behind the earth retaining wall indicated that the surrounding ground was not significantly disturbed.

Acknowledgments The authors would like to express their sincere thanks to the JR West Japan Railway Company for their support, comments, and suggestions.

Appendix 1: Elasto-viscoplastic constitutive model for clay considering structural changes

For the constitutive model for clay, an elasto-viscoplastic model which considers structural changes is used. The model is an over-stress type of viscoplasticity theory considering the material instability brought about by microstructural changes in the geomaterials [10].

The deviatoric and volumetric viscoplastic strain rates are given by

$$\dot{e}_{ij}^{vp} = C_{01}\exp\left\{m'\left(\bar{\eta}^* + \tilde{M}^*\ln\frac{\sigma'_m}{\sigma'_{\mathrm{mb}}}\right)\right\}\frac{\eta^*_{ij}-\eta^*_{ij(0)}}{\bar{\eta}^*} \tag{5}$$

$$\dot{\varepsilon}_{\mathrm{kk}}^{vp} = C_{02}\exp\left\{m'\left(\bar{\eta}^* + \tilde{M}^*\ln\frac{\sigma'_m}{\sigma'_{\mathrm{mb}}}\right)\right\}\left\{\tilde{M}^* - \frac{\eta^*_{mn}\left(\eta^*_{mn}-\eta^*_{mn(0)}\right)}{\bar{\eta}^*}\right\} \tag{6}$$

$$\bar{\eta}^* = \left\{\left(\eta^*_{ij}-\eta^*_{ij(0)}\right)\left(\eta^*_{ij}-\eta^*_{ij(0)}\right)\right\}^{1/2}, \quad \eta^*_{ij} = S_{ij}/\sigma'_m \tag{7}$$

$$C_{ijkl} = a\delta_{ij}\delta_{kl} + b(\delta_{ik}\delta_{jl}+\delta_{il}\delta_{jk}), \quad C_{01} = 2b, \quad C_{02} = 3a+2b$$

where $\dot{e}_{ij}^{vp}$ is the deviatoric viscoplastic strain rate tensor, $\dot{\varepsilon}_{\mathrm{kk}}^{vp}$ is the viscoplastic volumetric strain rate, σ'_m is the mean effective stress, C_{01}, C_{02}, and m' are viscoplastic parameters, $\bar{\eta}^*$ is the relative stress ratio, η^*_{ij} is the stress ratio tensor, subscript (0) indicates the initial state, *Sij* is the deviatoric stress tensor, $\tilde{M}^*$ is the dilatancy coefficient, *fp* is the plastic potential function, σ'_{ij} is the effective stress tensor, and σ'_{mb} is a hardening–softening parameter given as follows:

$$\sigma'_{\mathrm{mb}} = \sigma'_{\mathrm{ma}}\exp\left(\frac{1+e}{\lambda-\kappa}\varepsilon_{kk}^{vp}\right) \tag{8}$$

$$\sigma'_{\mathrm{ma}} = \sigma'_{\mathrm{maf}} + (\sigma'_{\mathrm{mai}} - \sigma'_{\mathrm{maf}})\exp(-\beta z) \tag{9}$$

$$z = \int_0^t \dot{z}\mathrm{d}t, \quad \dot{z} = (\dot{\varepsilon}_{ij}^{vp}\dot{\varepsilon}_{ij}^{vp})^{1/2} \tag{10}$$

where σ'_{maf} and σ'_{mai} are the final and the initial values of structural parameter σ'_{ma}, respectively, β is a parameter denoting the rate of degradation of the structure, e is the void ratio, λ is the compression index, κ is the swelling index, and. z is an accumulation of the second invariant of viscoplastic strain rate $\dot{\varepsilon}_{ij}^{vp}$.

From the above equations, it is seen that the decrease in σ'_{mb} in Eq. (8) can lead to softening behaviour and that Eq. (6) can describe the positive dilatancy depending on the stress ratio.

In the above formulation, no pure elastic region is taken into consideration although the over-stress type elasto-viscoplasticity can, in general, include the elastic region. However, in the present analysis, the viscoplastic

parameters C_{01} and C_{02} are small as 10^{-11}/s. Hence the effect of the elastic region is negligible even for the unloading process.

Appendix 2: Soil–water-coupled finite element method

For the numerical simulation, we use a finite element method for two-phase mixtures based on the finite deformation theory. In general the strain level in the analysis is not high in the whole domain but locally the strain may be not so small since the ground deformation may includes strain localization. In addition, the strain level induced in the construction activity cannot be known before analysis, and the finite deformation analysis is sufficient in general, but the small strain analysis is not. Based on the above consideration, we have used a finite deformation theory in the present analysis.

Biot's type of two-phase mixture theory is adopted to give the governing equations of the soil–water coupling problem (e.g., [13, 15]. An updated Lagrangian method with the objective Jaumann rate of Cauchy stress is used for the weak form of the rate type of equilibrium equations for the soil–water whole mixture which is given by the following equation:

$$\int_V \mathrm{div}\,\dot{\boldsymbol{S}}_{\boldsymbol{t}} \cdot \delta \boldsymbol{v} = 0 \tag{11}$$

$$\dot{\boldsymbol{S}}_{\boldsymbol{t}} \equiv \dot{\boldsymbol{T}} + \boldsymbol{T}\,\mathrm{tr}\boldsymbol{L} - \boldsymbol{T}\boldsymbol{L}^{\mathrm{T}} \tag{12}$$

in which $\delta \boldsymbol{v}$ is the virtual velocity vector, $\dot{\boldsymbol{S}}_{\boldsymbol{t}}$ is the nominal stress rate tensor, $\boldsymbol{T}$ denotes the Cauchy stress tensor, $\boldsymbol{L}$ denotes the velocity gradient tensor, and the superimposed dots indicate the time differentiation.

For the fluid phase, the weak form of the continuity equation is employed. The types of elements used in the three-dimensional analysis are eight-node isoparametric elements with a reduced Gaussian (2 × 2) integration for the soil skeleton and four-node isoparametric elements with a full (2 × 2) integration for the pore fluid. Detailed formulations of the equilibrium equation and the continuity equation can be found in the references, e.g., Oka et al. [13] and Higo et al. [6, 7].

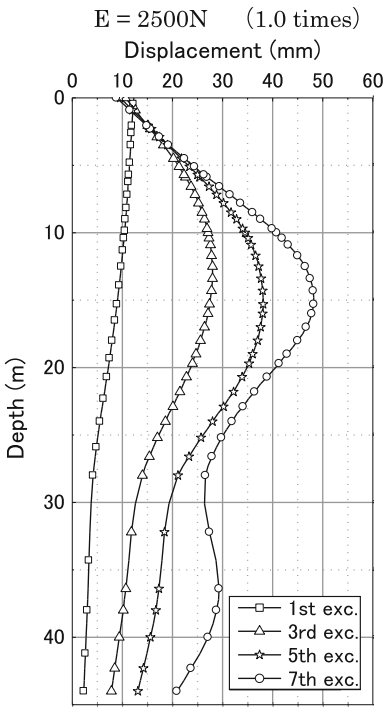

Fig. 18 Displacement of the retaining wall (E = 2500 N)

Appendix 3

The results of the parametric study are illustrated in the Figs. 18, 19, 20, 21, 22 and 23. The results show that the present value for E is reasonable considering the displacement of the retaining wall and the deformation of soil. Hence, considering the recommendation by RTRI (16) and the parametric study on E, we have adopted a Young's modulus which is 1.5 times larger for the Dg1 layer and

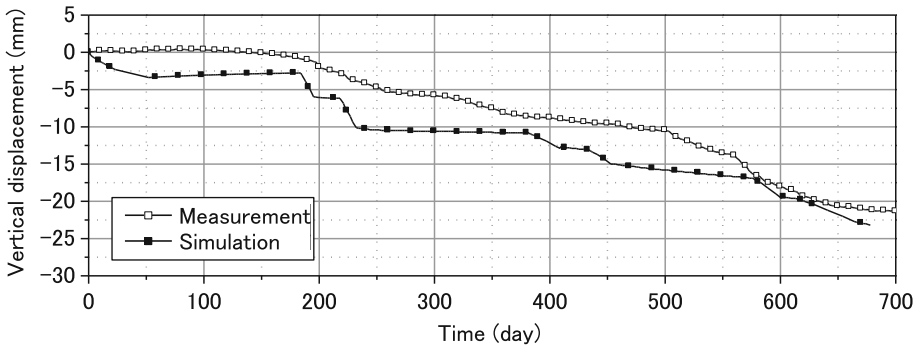

Fig. 19 Vertical settlement–time profile at a depth of GL-2.5 m behind the retaining wall (E = 2500 N)

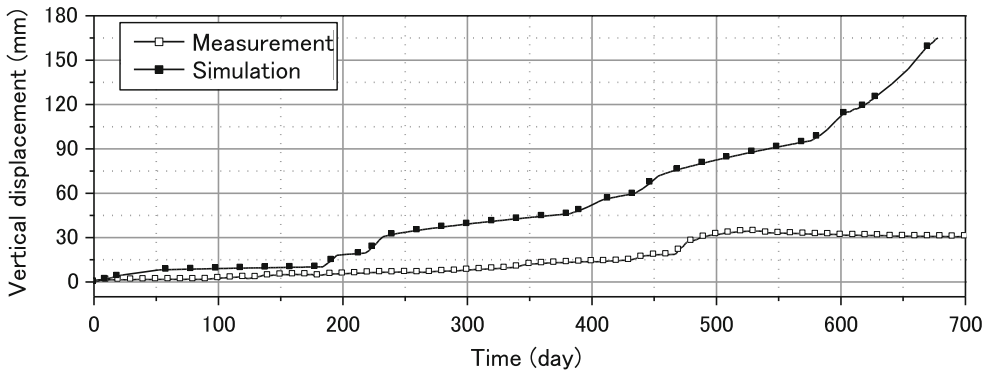

Fig. 20 Vertical settlement–time profile at a depth of GL-20.7 m in the excavation area ($E = 2500$ N)

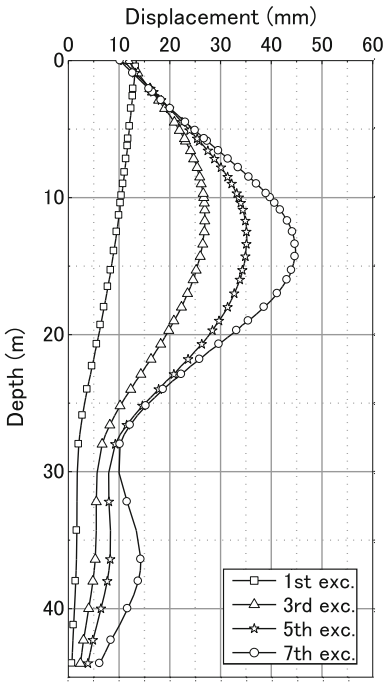

Fig. 21 Displacement of the retaining wall ($E = 3 \times 2500$ N)

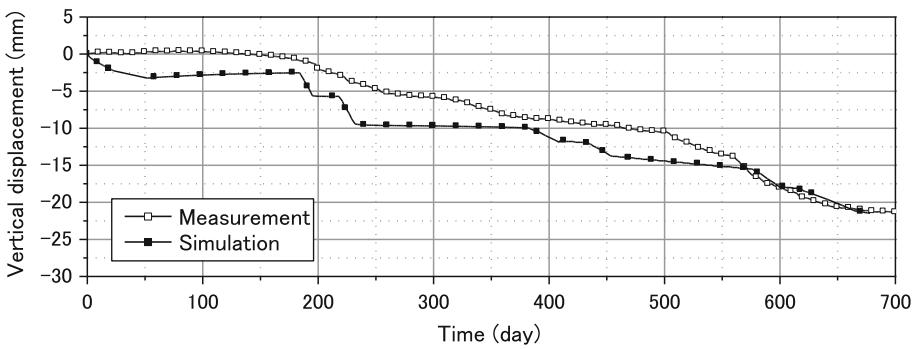

Fig. 22 Vertical settlement–time profile at a depth of GL-2.5 m behind the retaining wall ($E = 3 \times 2500$ N)

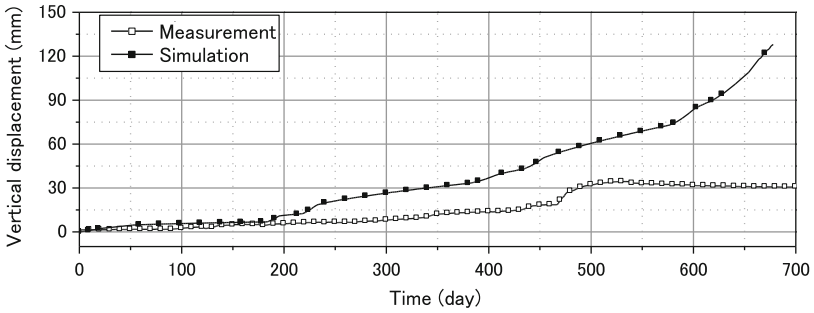

Fig. 23 Vertical settlement–time profile at a depth of GL-20.7 m in the excavation area ($E = 3 \times 2500$ N)

one which is 2.0 times larger for the Dg2 layer, which is consistent with the fact that the Pleistocene gravel layers are stiff and the expected strains are small.

References

1. AIJ (Architectural Institute of Japan) (2006) Symposium on various problems of design of the earth retaining wall. Committee report (Estimation of the effect of neighboring construction and countermeasure) (in Japanese)
2. Boonlert S, Oka F, Kimoto S, Kodaka T, Higo Y (2007) Elasto-viscoplastic finite element study of the effect of degradation on bearing capacity of footing on clay ground. Geomech Geoeng 2(4):235–251
3. Brown PT, Booker JR (1985) Finite element analysis of excavation. Comput Geotech 1:207–220
4. Building Center of Japan (2002) Revised version of the guide line for the design of soil improvement of building and its quality control, deep and shallow mixing method using cement type solidification material. Showa Jyoho Process **(in Japanese)**
5. Finno RJ, Blackburn JT (2007) Three-dimensional effects for supported excavations in clay. J Geotech Geoenviron Eng 133(1):1, 30–36
6. Higo Y, Oka F, Nagaya J, Watanabe T (2006a) Relationship between strain rate sensitivity and secondary compression coefficient. In: Proceedings of the 61st annual meeting of JSCE, vol 262, pp 519–520 (in Japanese)
7. Higo Y, Oka F, Kodaka T, Kimoto S (2006) Three-dimensional strain localization of water-saturated clay and numerical simulation using an elasto-viscoplastic model. Philos Mag 86(21–22):3205–3240
8. Japan Architecture Center (2002) Revised version: design of improved ground for building and guideline for quality control-deep and shallow mixing method using cement solidification material. Shyowa Jyoho Process Co
9. Karim MR, Oka F, Krabbenhoft K, Leroueil S, Kimoto S (2013) Simulation of long-term consolidation behavior of soft sensitive clay using an elasto-viscoplastic constitutive model. Int J Numer Anal Methods 37:2801–2824
10. Kimoto S, Oka F (2005) An elasto-viscoplastic model for clay considering destructuralization and consolidation analysis of unstable behavior. Soils Found 45(2):29–42
11. Leroueil S, Samson L, Bozozuk M (1983) Laboratory and field determination of preconsolidation pressures at Gloucester. Can Geotech J 20(3):477–490
12. Mukai H (2009) Deformation analysis of earth-retaining wall and ground induced by the open cut construction. Ph D. Thesis, Kyoto University (in Japanese)
13. Oka F, Higo Y, Kimoto S (2002) Effect of dilatancy on the strain localization of water-saturated elasto-viscoplastic soil. Int J Solids Struct 39(13–14):3625–3647
14. Oka F, Higo Y, Nakano M, Mukai H, Izunami T, Kakeda S, Amano K, Nagaya J (2009) Deformation analysis of earth-retaining wall during excavation of Nakanoshima soft clay deposit by an elasto-viscoplastic finite element method. JSCE J Geotech Geoenviron Eng C 65(2):492–505 **(in Japanese)**
15. Oka F, Kimoto S (2012) Computational modeling of multiphase geomaterials. CRC press, Taylor & Francis Group, Boca Raton, FL, USA
16. Railway Technical Research Institute of Japan (2001) Standard for design of railway structures and interpretation, open-cut tunnel. Maruzen Co., 59–64 and Referential material No. 11, Real rebound and its calculation examples. Maruzenn Co., 429–436 (in Japanese)
17. Railway Technical Research Institute of Japan (2004) Standard for design of railway structures and interpretation, concrete structures. Maruzen Co., 79 (in Japanese)
18. Takada N (2012) Elasto-viscoplastic analysis of large scaleexcavation of soft clay depositconsidering soil improvement. Ph. D. Thesis, Kyoto University (in Japanese)
19. Tanaka H (1994) Behavior of a braced excavation in soft clay and the undrained shear strength for passive earth pressure. Soils Found 34(1):53–64
20. Uto K (1967) Sounding of ground, foundations of structures. Kansai Branch of Japan Society of Testing Materials, pp 33–66 (in Japanese)
21. West Japan Railway Company, JR West Japan Consulting Company and Joint venture group for the construction and improvement of Osaka Station (2011) Report of Technical Committee of Construction and Improvement for Osaka Station, May 2011 (in Japanese)
22. Whittle AJ, Davies RV (2006) Nicoll highway collapse: evaluation of geotechnical factors affecting design of excavation support system. In: Proceedings of international conference on deep excavations, 28–30 June 2006, Singapore, pp 1–16